

pubs.acs.org/JACS Article

Immune-Induced Antibody—DNA Hybrid Condensates

Sara Scalia, Marco Cappa, Lorenzo Rovigatti, Erica Del Grosso,* and Francesco Ricci*



Cite This: https://doi.org/10.1021/jacs.5c13855



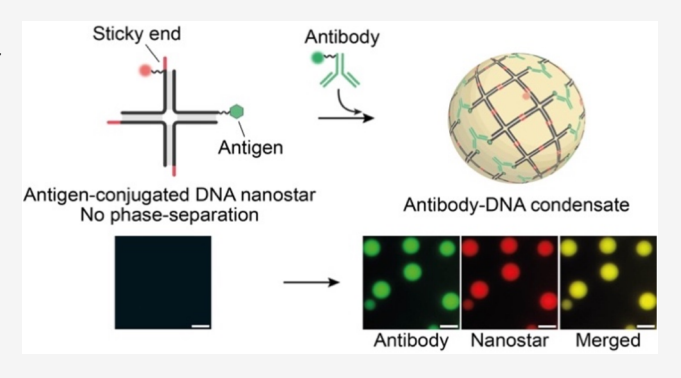
ACCESS I

Metrics & More

Article Recommendations

SI Supporting Information

ABSTRACT: We report here the combined use of Watson—Crick and antibody—antigen interactions to induce phase separation of antibody—DNA hybrid condensates. To achieve this, we have used an antigen-conjugated star-shaped DNA motif (nanostar) in which three arms terminate with single-stranded DNA sticky ends while the fourth arm is end-conjugated with a moiety (i.e., an antigen) that can be recognized by a specific bivalent antibody. Through the concerted action of selective Watson—Crick base-pairing between the sticky ends and bivalent antibody—antigen binding, such antigen-conjugated nanostars phase-separate to form micron-scale hybrid condensates with structural stability provided by both nucleic acids and antibodies. We have demonstrated the specific and orthogonal antibody-induced phase separation of four different



antigen-conjugated nanostars (biotin, DIG, DNP and MUC1), each with their corresponding antibody. By adding increasing concentrations of the specific antibody to a fixed concentration of antigen-conjugated nanostars (300 nM), we observe concentration-dependent formation of antibody—DNA condensates, starting at low nanomolar levels of the antibody. The antibody—DNA hybrid condensates are also reversible and can be cyclically formed/dissolved by the cyclic degradation/addition of the specific antibody. We qualitatively (and in some cases quantitatively) reproduce these results with an approach that conjugates theory and simulations of a phase-field model. The introduction of antibody—antigen interactions into the phase separation process of DNA brings these systems closer to natural cellular systems that rely on intricate networks of protein—protein or protein—nucleic acid interactions and allows for greater programmability and versatility that could have applications in sensing and drug delivery.

■ INTRODUCTION

The field of nucleic acid nanotechnology has rapidly advanced in recent years, paving the way for the development of innovative materials and biomolecular structures that employ the programmable nature of nucleic acid interactions. ^{1,2} One emerging area involves the possibility of creating DNA or RNA-based condensates, assemblies of synthetic nucleic acids that exhibit liquid-like behavior and highly programmable phase separation features. ^{3–14} DNA/RNA condensates have attracted considerable attention as synthetic analogues of natural cells or membraneless compartments, offering a platform for studying and engineering biomolecular processes in a controlled, customizable environment with potential applications in various fields, including biophysics, ^{9,14–22} materials science ^{18,23–26} and bioengineering. ^{27–32}

In order to increase the diversity and complexity of such nucleic acid-based condensates, several examples have recently been reported in which the incorporation of other molecules into the condensates has been demonstrated by exploiting the programmability and versatility of nucleic acids. For example, the incorporation of proteins using aptamers or ligands embedded in DNA/RNA condensates has been demonstrated as a way to improve the biomimetic properties of nucleic acid condensates.^{9,32–34} Alternatively, the introduction of specific

enzymatic substrates into the condensates was used as a way to provide localized enzymatic activity^{27,35-38} and to enable the spatial and temporal control of biomolecular interactions within the condensates.³⁵

While the above examples clearly highlight the possibility of extending the functionality and versatility of DNA/RNA condensates to enable the creation of biomimetic structures, they lack a general feature that characterizes natural cellular compartments. That is, in nature, membraneless organelles and cellular condensates often form through intricate networks of protein—protein or protein—nucleic acid interactions that lead to dynamic and regulated assemblies of complex biomolecular structures. ^{39,40} In other words, condensation in nature is often the result of concerted interactions that ultimately enable complex spatial organization and functionality so that specific biochemical reactions, signal transduction pathways and cellular processes can take place. ^{41–46} However, DNA- and

Received: August 11, 2025 Revised: October 7, 2025 Accepted: October 9, 2025



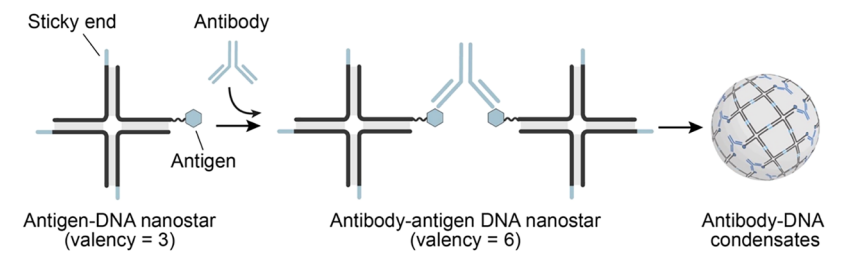


Figure 1. DNA-based condensates formed by Watson–Crick and antibody–antigen interactions. Schematic representation of the antigenconjugated DNA nanostar. The four-armed nanostar is designed to have three arms ending with a 6-nt sticky end and the fourth arm chemically conjugated at the 5' end with an antigen. The nanostar is designed so that phase separation into antibody–DNA hybrid condensates occurs only through the concerted action of base-pairing between the sticky ends and bivalent antibody binding that joins two antigen-conjugated DNA nanostars.

RNA-based condensates have so far mainly relied on the formation of specific nucleic acid base pairs or on nonspecific interactions (e.g., electrostatic interactions or hydrophobic interactions have shown phase separation. Only a few examples have shown phase separation of mixed DNA—peptide coacervates, and these are induced by nonspecific electrostatic interactions. This ultimately limits the programmability and versatility of these tools. A similar lack of diversity in the phase separation process also exists in synthetic protein-based biomolecular condensates, which are usually prepared using engineered proteins that have intrinsically disordered regions and can only form weak, nonspecific interactions. ^{49,50}

Motivated by the above considerations, in an attempt to mimic the diverse array of molecular interactions that occur in natural cellular systems, we report here the combined use of Watson-Crick and specific antibody-antigen interactions to induce phase separation of antibody-DNA hybrid condensates. The immune-induced phase separation strategy we used here is based on star-shaped DNA motifs (i.e., nanostars) designed to have three DNA-based sticky ends and one antigen at the ends of their four arms. Under our experimental conditions, phase separation of such nanostars occurs only through the combined effect of selective base-pairing between the sticky ends and bivalent antibody-antigen binding, resulting in hybrid condensates with structural stability provided by both nucleic acids and antibodies. The introduction of an additional level of control over the phase separation process allows for greater programmability and versatility in synthetic biomolecular condensates.

■ RESULTS AND DISCUSSION

To achieve immune-induced phase separation of antibody—DNA hybrid condensates, we used star-shaped DNA motifs, also known as DNA nanostars, which can spontaneously self-assemble under certain experimental conditions to form DNA-rich condensates. The ability of the nanostars to phase separate, as well as the stability and size of the resulting condensates, are influenced by the number, length, and strength of their sticky ends. ^{6,8,51–54} In this work, we employed DNA nanostars with four 6-nt sticky ends (valency = 4), optimized by Saleh and co-workers. ⁹ We replaced one of the four sticky ends of the nanostar with a molecule (i.e., an antigen) that can be recognized by a specific antibody. When such antigen-conjugated nanostars are mixed in a solution at submicromolar concentrations, their reduced valency prevents them from spontaneously separating. After addition of a specific antibody that leads to bivalent binding of two antigen-

conjugated nanostars and formation of an antibody-DNA hybrid nanostar with an effective valency of 6, phase separation can instead occur spontaneously (Figure 1). To demonstrate this, we first used biotin as an antigen and conjugated it to the 5'-end of one of the four oligonucleotides that form the nanostar (Figure 2a). We then tested the phase separation of such biotin-conjugated nanostars (at 300 nM) in the absence and presence of a stoichiometric concentration of anti-biotin IgG antibody (i.e., 150 nM). To monitor the formation of condensates, we labeled one of the four arms of the nanostar with a fluorophore (e.g., Cy3) and also used a fluorophorelabeled anti-biotin antibody (e.g., AF647) (Figure 2a). Under these conditions, we were able to observe micron-scale condensates as early as 1 h after addition of the anti-biotin antibody, while in the absence of the antibody no condensates were observed even after 72 h (Figures 2b and S1, and Supporting Video 1). Remarkably, the microscopy images obtained at the Cy3 (nanostar) and AF647 (antibody) channels show a homogeneous distribution and almost perfect colocalization of the antibody and nanostar (Figure 2c,d). Similar colocalization is also observed through z-stack acquisition using confocal microscopy (Figure S2, and Supporting Video 2), once again supporting the hypothesis that the condensates are formed by the concerted role of DNA-DNA and antibody-antigen interactions.

Further confirmation of this is also provided by control experiments in which we first replaced the bivalent anti-biotin antibody with a monovalent anti-biotin Fab fragment that is unable to bridge two nanostars after binding to biotin (Figure 2e). As expected, in this case we did not observe any visible condensate even 72 h after the addition of the anti-biotin Fab fragment (Figure S1). Similar results were observed when nonspecific bivalent antibodies were used (Figures 2e and S1). The final proof of the role of bivalent binding of the antibody as a driving force for phase separation comes from an additional control experiment in which we used only DNA-DNA interactions. More specifically, we redesigned the antigen-conjugated DNA nanostar described above to replace the antigen with a 14-nt DNA anchor sequence (Figure S3). We then added a synthetic DNA duplex in solution that mimics an antibody and flanks two identical 14-nt DNA domains that are complementary to the anchor sequence in the nanostar. Binding of such a DNA-based antibody mimic rapidly leads to phase separation of the nanostars (Figure S3), again supporting the hypothesis that the valence enhancement induced by the bivalent binding is crucial for the observed phenomenon. Of note, the average density values of DNA condensates and antibody-DNA condensates are within

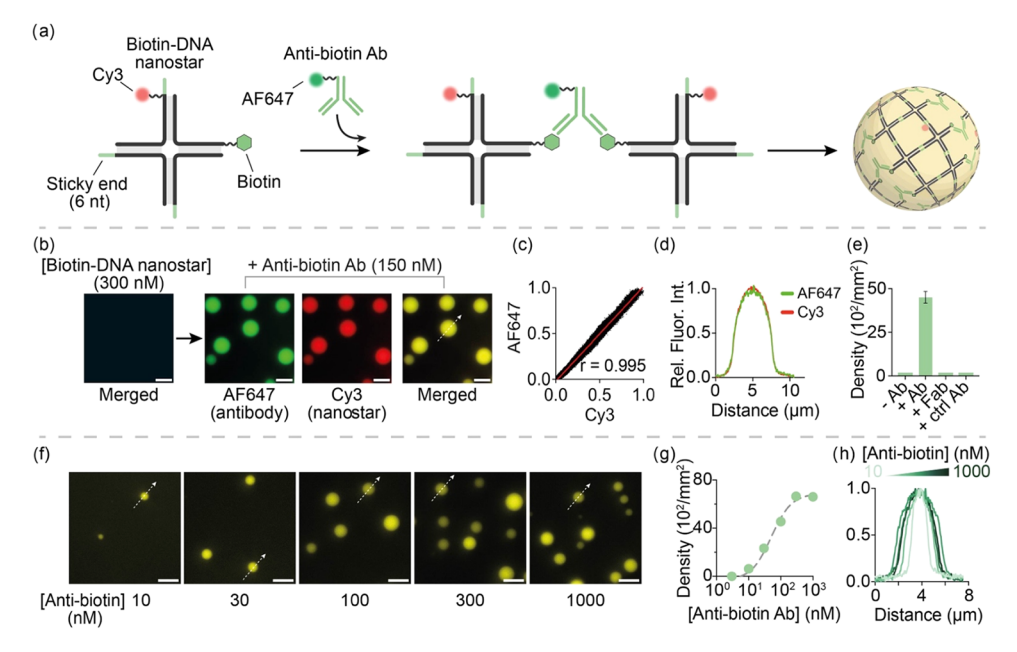


Figure 2. Phase separation of antibody-DNA hybrid condensates through the formation of a biotin and anti-biotin antibody complex. (a) Schematic representation of biotin-DNA nanostars (labeled with Cy3 fluorophore) that phase-separate into condensates only in the presence of anti-biotin antibody (labeled with AF647 fluorophore). (b) Epifluorescence micrographs of biotin-DNA nanostars (300 nM) in the absence and presence of anti-biotin antibody (150 nM). (c) Scatter plot of the measured pixel intensity showing the correlation (Pearson's correlation coefficient, r) of Cy3 (biotin-DNA nanostar) and Alexa 647 (anti-biotin antibody) fluorophores in the sample containing antibody-DNA hybrid condensates. (d) Graph showing fluorescence intensity line plots of labeled biotin-DNA nanostars and anti-biotin antibody along the dashed line in the adjacent microscope image (merged). (e) Condensates' density values (count/mm²) obtained without anti-biotin antibody, with anti-biotin antibody, with anti-biotin monovalent Fab fragment and with control nonspecific antibodies (anti-Dig, anti-DNP or anti-MUC1). (f) Epifluorescence micrographs (merged channels) of antibody-DNA hybrid condensates at different anti-biotin antibody concentrations. (g) Plot of condensates' density vs anti-biotin antibody concentration. The dashed gray line represents the fit to the theoretical data, rescaled to match the absolute value of the experimental points (see Figure S8). (h) Graph showing fluorescence intensity line plots of the labeled anti-biotin antibody along the dashed line in adjacent microscope images (merge). For each condition, we considered representative condensates with an area corresponding to the average area of the sample. Experiments were performed in 10 mM Tris HCl and 0.5 M NaCl, pH 7.5 buffer at T = 25 °C. Microscopy images were taken 1 h after the addition of the antibody. All scale bars of the micrographs are 5 µm. Specificity experiments were performed adding anti-biotin Fab fragments and control antibodies at 150 nM. All the data in this figure correspond to the mean values obtained from three replicates; error bars are the standard deviation of the mean.

experimental error of each other ($(13.7 \pm 0.9) \times 10^2/\text{mm}^2$ for DNA condensates vs (12.8 ± 1.4) × $10^2/\text{mm}^2$ for antibody—DNA condensates), indicating a very efficient condensation process even in the presence of a large moiety as the antibody (Figure S3). Despite this, the average area of the DNA condensates ($47.6 \pm 0.9 \ \mu\text{m}^2$) is about 2-fold larger than that of antibody—DNA condensates ($27.3 \pm 0.4 \ \mu\text{m}^2$), probably due to a poorer tendency of antibody—DNA condensates to coalesce (Figure S3).

The combined effect of antibody-antigen and DNA-DNA interactions in condensate formation is quite delicate. For example, replacing additional sticky ends with more antigens results in the loss of the nanostars' ability to phase condense (Figure S4), likely due to the possibility of bivalent binding of the same antibody to a single nanostar or to the formation of kinetically trapped states induced by overly strong antibody binding. Also, reducing the number of sticky ends and retaining an antigen on the nanostar greatly reduces its ability to phase separate (Figure S4). We also investigated the dynamic nature of our system. To do this, we first prepared antibody-DNA hybrid condensates using Cy5-labeled biotin-DNA nanostars and anti-biotin antibody and then added Cy3labeled DNA nanostars (300 nM) with the same sticky ends but without the antigen and observed their integration into the pre-existing condensates (Figure S5). We speculate that the unconjugated DNA nanostars integrate into the condensates

through exchange with antigen-conjugated nanostars that are not linked to an antibody. We then repeated the experiment but this time added Cy3-labeled biotin-conjugated DNA nanostars with a different set of sticky ends to a solution of Cy5-labeled anti-biotin antibody—DNA condensates. In this case, we observed the formation of a separate set of condensates containing only Cy3-labeled nanostars, likely due to phase separation induced by anti-biotin antibodies still free in solution. Interestingly, we observed that the condensates tend to connect, forming regular "chains" of alternating condensates, suggesting the ability of antibodies to bridge different condensates through bivalent binding (Figure S6).

The immune-induced phase separation of antibody—DNA hybrid condensates is concentration-dependent and extremely sensitive. To demonstrate this, we used a fixed concentration of biotin—DNA nanostars (i.e., 300 nM) and added increasing concentrations of anti-biotin antibody, observing an initial concentration-dependent increase in condensate density, which then levels off at around 300 nM (Figure 2f—h). A similar antibody concentration dependence is also observed for the condensate diameter. Moreover, consistent with the polydisperse nature of such droplets, the diameter distribution for each experiment is quite large (Figure S7). We also note that antibody—DNA hybrid condensates can be observed upon addition of an anti-biotin antibody concentration as low as 10

nM, suggesting that a similar approach may be useful for sensing applications.

All the trends observed in experiments are qualitatively captured by a theoretical model that takes into account the binding specificity of both nanostars and antibodies, their valence and their effective excluded volume in a mean-field fashion. 54,55 Notably, the theory reproduces the experimentally observed phase boundaries semiquantitatively (Figure S8), despite containing no free parameters, since all inputs are fixed to values obtained from numerical simulations or established models. We couple the theory to a numerical phase-field approach based on the Cahn-Hilliard equation⁵⁵ to investigate the concentration dependence of the condensate's density. This integrated theoretical-numerical framework reproduces the experimental trends at a qualitative rather than quantitative level (Figure S9), a result consistent with its mean-field character and the absence of microscopic detail. In addition, the theory can also be used to fit the experimental results of Figure 2g to obtain the concentration dependence of the condensate's surface tension (Figure S10).

The immune-induced phase separation of antibody-DNA hybrid condensates is a versatile, modular and orthogonal process. We re-engineered different DNA nanostars and conjugated each of them with a different antigen to induce discrete phase separation with different specific antibodies. We first demonstrated this by conjugating a new antigen (in this case digoxigenin, Dig) to one of the nanostar-forming oligonucleotides and using the anti-Dig antibody as the driver for the phase separation process (Figure 3a). Also in this case, we observed visible condensates only in the presence of anti-Dig antibodies and in a concentration-dependent manner with sensitivity and specificity similar to those observed with the biotin/anti-biotin system (Figures 3a and S11). Similar results were also obtained using dinitrophenol (DNP) as antigen and anti-DNP antibody as input antibody, although with slightly poorer sensitivity (Figures 3b and S12) and with overall lower condensate density compared to the other antibody-antigen pairs. We attribute this difference to the fact that the anti-DNP antibodies used here are IgE antibodies, which have important structural differences compared to IgG antibodies (anti-biotin, anti-Dig, anti-MUC1). For example, IgE antibodies lack the classical hinge region of IgG antibodies and contain an additional constant domain in each heavy chain, resulting in reduced flexibility of the Fab regions.⁵⁶ In addition, IgEs exhibit higher levels of glycosylation compared to IgGs. 57 All these factors may contribute to differences in the efficiency of the immune-induced phase separation process. We also programmed a modular version of the same immune-induced phase separation by redesigning the nanostars to have three 6nt sticky ends and a 17-nt anchor strand that allows hybridization of a complementary antigen-conjugated oligonucleotide. This approach is particularly advantageous for easily exchanging the antigen on the nanostar so that it can respond to different antibodies. For such a modular version, we used as antigen a peptide with 15 residues excised from the MUC1 protein which is recognized by the clinically relevant anti-MUC1 antibody (Figure 3c). Also in this case, the modular version of the nanostar showed immune-induced phase separation with sensitivity and specificity comparable to those of their nonmodular counterparts (Figures 3c and S13). We also tested EGFR protein as the antigen in this modular format. In this case, however, we observed the formation of DNA condensates not only in the presence of the

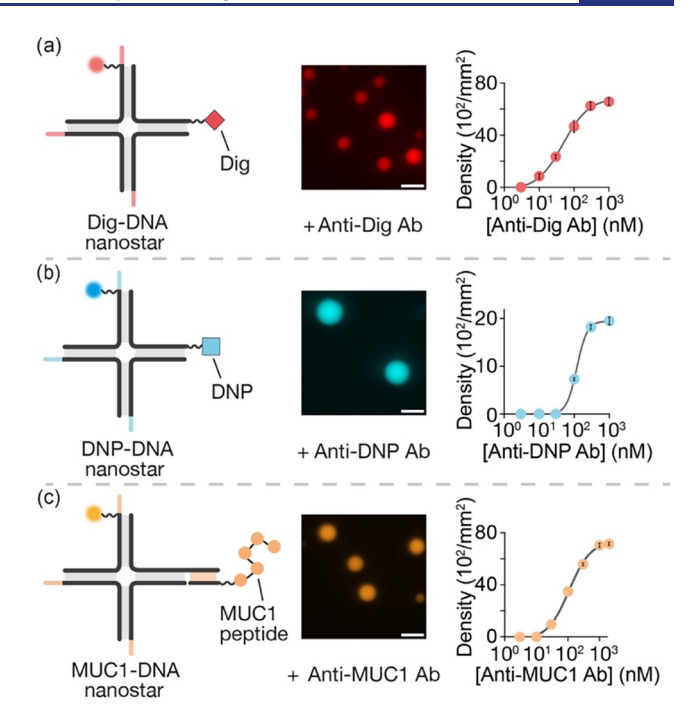


Figure 3. Phase separation of antibody—DNA hybrid condensates using different antibody—antigen pairs. In each row are depicted (left) the schematic of the four-armed DNA nanostars, each conjugated with a different antigen; (center) the epifluorescence micrograph of antigen-conjugated DNA nanostars (300 nM) in the presence of the specific antibody (150 nM); and (right) a plot of the condensate's density vs the specific antibody concentration. Antibody—antigen pairs used here are (a) Dig and anti-Dig antibody, (b) DNP and anti-DNP antibody and (c) MUC1 peptide and anti-MUC1 antibody; experiments were performed in 10 mM Tris HCl and 0.5 M NaCl, pH 7.5 buffer at $T=25\,^{\circ}$ C. Microscopy images were taken 1 h after the addition of the specific antibody. All scale bars of the micrographs are 5 μ m. All the data in this figure correspond to the mean values obtained from three replicates; error bars are the standard deviation of the mean.

specific antibody (Cetuximab) but also when nonspecific antibodies were added (i.e., anti-DNP, anti-Dig and antibiotin) (Figure S14). Further investigation of this unexpected result revealed that the nonspecific phase separation process does not directly involve the nonspecific antibody, which is not colocalized in the condensate formed (Figure S15). Instead, it is likely due to sodium azide, a common ingredient present in all the antibody solutions tested (Figure S16). We hypothesize that sodium azide might induce a structural change in the EGFR protein, triggering its dimerization s18,59 and consequent phase condensation, but at this stage no experimental confirmation of this hypothesis is available.

Since the sticky ends of the antigen-conjugated nanostars shown above have different sequences and the antibody—antigen interactions are highly specific, the immune-induced phase separation process is a completely orthogonal process that can occur in the same solution without cross-reactivity. To demonstrate this, we mixed in the same solution three different nanostars, each conjugated to a different antigen (biotin, Dig and DNP) and labeled with non-overlapping orthogonal fluorophores (Cy5, Cy3 and FAM, respectively) (Figure 4a). We then added to this mixture the three input antibodies (antibiotin, anti-Dig and anti-DNP antibodies) in different combinations and observed orthogonal phase separation of

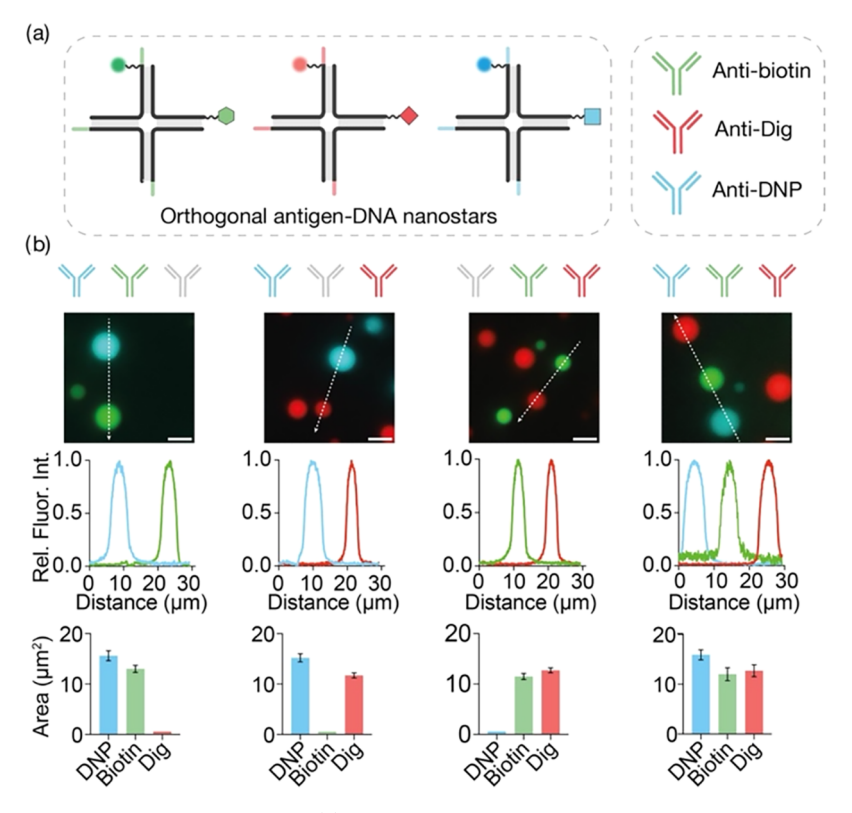


Figure 4. Orthogonal antibody—DNA hybrid condensates. (a) Scheme showing the three orthogonal antigen-conjugated DNA nanostars with different sticky end sequences, each responsive to a different antibody and labeled with a different fluorophore. (b) (Top) Merged epifluorescence microscopy images obtained by adding each antibody in different combinations (colored antibodies on top of each microscopy image represent the antibodies added). (Center) Fluorescence intensity line plots of the labeled antigen-conjugated DNA nanostars along the dashed line indicated in merged microscope images. (Bottom) Bar plots showing the average condensate area measured for each fluorophore. Experiments were performed in 10 mM Tris HCl and 0.5 M NaCl, pH 7.5 buffer at T = 25 °C. Microscopy images were taken 1 h after the addition of the relevant antibodies. All scale bars are 5 μ m. All the data in this figure correspond to mean values obtained from three replicates; error bars are the standard deviation of the mean.

the fully discrete condensate only in the presence of the corresponding specific input antibody (Figure 4b and S17).

The introduction of an additional molecular interaction into the phase separation process allows for greater programmability in the formation and dissolution of the antibody-DNA hybrid condensates. We first demonstrate here the possibility of inducing the dissolution of antibody-DNA hybrid condensates by adding free antigen in solution that competes for antibody binding (Figure 5a). By doing so, we observe a strong reduction in the area of the condensates, although without complete dissolution (Figure 5b-d), probably due to the fact that the free antigen is not able to completely overcome the avidity effect caused by the bivalent binding of the antibody in the condensates. As an alternative approach to induce input-dependent dissolution of the hybrid condensates, we used papain, a proteolytic enzyme that degrades IgG antibodies into Fab and Fc fragments (Figure 5e). In this case, we used biotin-DNA nanostars and anti-biotin antibodies and observed papain concentration-dependent dissolution kinetics leading to complete dissolution of the condensates, supporting the assumption that antibody-antigen interactions are crucial for the structural stability of the condensates (Figure 5f). Remarkably, the addition of anti-biotin antibodies after papaininduced dissolution of the condensates leads to a transient formation of antibody-DNA hybrid condensates, as the kinetics of the phase transition is faster than that of papaininduced enzymatic degradation (Figure 5g,h). The numerical

approach we developed qualitatively reproduces these findings (Supporting Video S3).

We also show that multiple antibodies can participate in the same phase separation process. To this end, we first engineered a four-armed DNA nanostar that has two sticky 6-nt ends on opposite arms and two different antigens (i.e., biotin and Dig) on the remaining arms (Figure S18). As expected, the reduced valency of such a nanostar does not allow efficient phase separation under our experimental conditions (nanostar concentration of 200 nM), and no condensates are observed in the absence of anti-biotin and anti-Dig antibodies. The addition of only one specific antibody (i.e., 100 nM each), which would lead to the formation of an antibody-nanostar complex with valency = 4, also does not result in any visible phase separation process, probably due the low concentration of antigen-conjugated nanostars used in this experiment (i.e., 200 nM). Only with the addition of both anti-biotin and anti-Dig antibodies can we observe efficient formation of antibody-DNA hybrid condensates showing colocalization of both antibodies (Figure S18).

CONCLUSION

Inspired by the diversity of molecular interactions used by natural systems to create membraneless organelles and cellular condensates, ^{39,40} we report here the programmable phase separation of antibody—DNA hybrid condensates induced by the combined use of sequence-specific Watson—Crick and

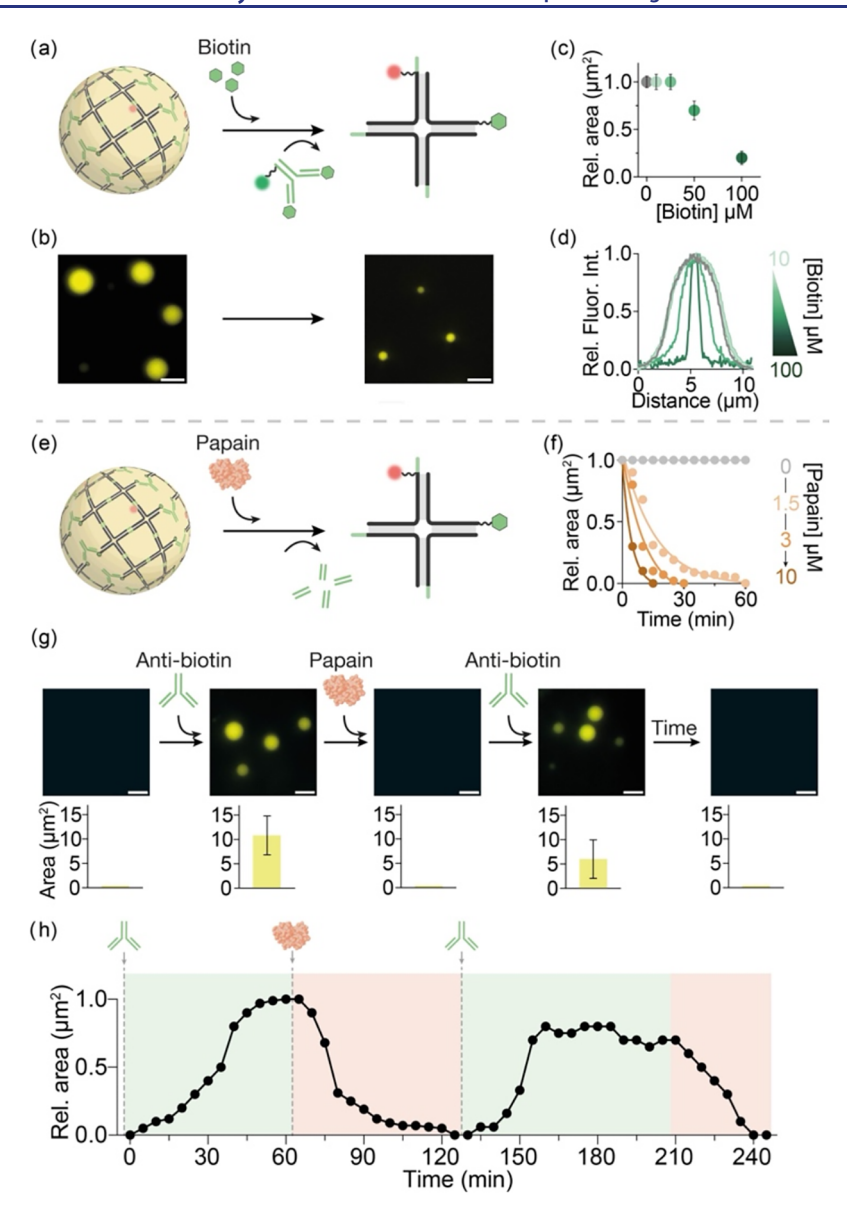


Figure 5. Programmable dissolution of antibody—DNA hybrid condensates. (a) Scheme of the antibody—DNA hybrid condensates' dissolution through competition with free antigen. (b) Epifluorescence microscopy images demonstrating the dissolution of biotin antibody—DNA condensates after the addition of free biotin (100 μM). (c) Plot of normalized average area vs the concentration of free biotin. (d) Fluorescence intensity line plot of the labeled anti-biotin antibody within hybrid condensates after the addition of varying free biotin concentrations. (e) Scheme of papain-driven biotin antibody—DNA hybrid condensates' dissolution. (f) Time-dependent plot of the normalized average area of antibody—DNA hybrid condensates with different degradation times by varying the concentration of papain. (g) (Top) Epifluorescence microscopy images of biotin antibody—DNA condensates after the cyclic addition of anti-biotin antibody and papain. (Bottom) Average area of condensates measured after each addition. (h) Time-dependent plot of the normalized average area of the antibody—DNA hybrid condensates after the cyclic addition of anti-biotin antibody and papain. Experiments were performed in 10 mM Tris HCl, 0.5 M NaCl, 15 mM Cysteine, pH 7.5 buffer at T = 25 °C. [Biotin—DNA nanostars] = 300 nM, [anti-biotin antibody] = 150 nM. Papain was added at a concentration of 1.5 μM, unless otherwise specified. All scale bars of the microscopy images are 5 μm. Data in panel c correspond to the mean values obtained from three replicates; error bars are the standard deviation of the mean.

selective antibody—antigen interactions. To this end, we have designed antigen-conjugated four-armed DNA nanostars that phase separate into micron-scale droplets only in the presence of the specific bivalent antibody that recognizes the antigen. Thanks to the specific nature of the interactions involved in the phase separation process, it is possible to rationally design different antigen-conjugated nanostars that undergo orthogonal phase separation in the presence of different antibodies. Such immune-induced phase separation also occurs as a function of antibody concentration, demonstrating the

possibility of utilizing a similar approach for sensing applications.

By incorporating a broader range of molecular inputs into DNA condensates, more complex and functional biomolecular structures can be created that closely mimic the complexity and dynamics of natural cellular systems. This multicomponent approach expands the scope of DNA nanotechnology and synthetic biology and offers new opportunities for the development of advanced biomaterials, bioinspired devices and biotechnological applications that take advantage of the

synergistic interactions among DNA, proteins, RNA and small molecules. The antibody-triggered, concentration-dependent phase separation, for example, can provide highly selective, multiplexed detection of biomarkers at low concentrations. Antibody-responsive condensates can also be employed to encapsulate and release therapeutic cargos in response to specific immune signals, enabling spatial and temporal control of drug availability. Finally, these hybrid condensates could enable the creation of dynamic biomimetic intracellular condensates, providing a platform to study natural phase separation processes or engineer novel cellular functions.

■ EXPERIMENTAL SECTION

Chemicals. All reagent-grade chemicals, including Trizma hydrochloride, Sodium chloride, Cysteine, biotin and digoxigenin were purchased from Sigma-Aldrich and used without further purifications. All buffer solutions were filtered through 0.22 μ m syringe filters (Millex), stored at 4 °C and used within 3 weeks of preparation. Papain (Carica papaya) was purchased from Merck (Darmstadt, Germany).

Antibodies. Goat polyclonal anti-digoxigenin antibody and goat polyclonal anti-biotin antibody were purchased from Vector Laboratories (USA), sheep polyclonal anti-Dig Fab fragment was purchased from Merck (Darmstadt, Germany) and goat polyclonal anti-biotin Fab fragment was purchased from Rockland (USA). AF647 mouse monoclonal anti-biotin antibody was purchased from Biotium (USA). AF488 goat polyclonal anti-Dig antibody was purchased from Vector Laboratories (USA). Mouse monoclonal anti-DNP antibodies were purchased from Sigma-Aldrich, (USA). Cetuximab, monoclonal Anti-MUC1 antibody and EGFR protein were kindly provided by Merck (Darmstadt, Germany).

Oligonucleotides. The sequences of the DNA oligonucleotide strands were modified from the 4-arm nanostars reported elsewhere. Oligonucleotides were synthesized, labeled and HPLC-purified by Metabion International AG (Planegg, Germany) and Biomers (Germany) and used without further purification. PNA/Peptide chimera probes were purchased from Panagene (South Korea). The oligonucleotides were shipped lyophilized and then dissolved in phosphate buffer 30 mM, pH 7.2 at a concentration of 100 μ M and stored at $-20~^{\circ}$ C until use. The sequences of all the oligonucleotide strands used are reported in the Supporting Information.

EGFR–DNA Hybrid Conjugation. Conjugation of DBCO-modified DNA strands to the protein EGFR was performed using ProFire (Dynamic Biosensors, Germany) and an amine coupling kit following the manufacturer's instructions. For that, 4 nmol of DNA was conjugated with 400 μ g of EGFR overnight. The cross-linking products were separated by ion exchange chromatography using the ProFire equipment, and after the data analysis with the equipment software, the fractions that correspond to 1:1 binding ratio were collected and stored at -20 °C.

Preparation of Antigen-Conjugated DNA Nanostars. All nanostars were formed by mixing each oligonucleotide at a final concentration of 15 μ M in a buffer consisting of 10 mM Tris-HCl (pH 7.5). To fluorescently label the nanostars, one of the strands was modified using a fluorescent dye, which was mixed at a 5% molar ratio in the solution. The mixture was placed in a Bio-Rad Mastercycler Gradient thermocycler, held at 95 °C for 5 min and then gradually cooled to room temperature at a rate of -0.2 °C/min. The assembled nanostars were subsequently stored at 4 °C for preservation. Each antigen—DNA nanostar was prepared separately. For nanostars with a modular design, they were first prepared as reported above using the four structural oligonucleotides and then incubated for 30 min with the EGFR- or MUC1-conjugated oligonucleotide (1:1 ratio) at room temperature.

Immune-Induced Formation of Antibody–DNA Condensates. Immune-induced formation of antibody–DNA hybrid condensates was achieved in 0.5 mL Eppendorf tubes by isothermally mixing antigen–DNA nanostars (or antigen-mimic DNA nanostars)

(300 nM), NaCl (0.5 M) and varying concentrations of a specific bivalent antibody (or synthetic antibody-mimic DNA duplex) in 10 mM Tris—HCl buffer (pH 7.5). Immediately after the addition of antibody, the mixture was incubated at 25 $^{\circ}\mathrm{C}$ for 1 h (unless otherwise indicated in the text) in a thermoshaker at 330 rpm in order to prevent condensate sedimentation.

Fluorescence Microscopy. Epifluorescence micrographs were obtained using a Zeiss Observer 7 inverted epifluorescence microscope equipped with a 100× oil immersion objective (EC Plan-Neo Fluor) and a monochrome Axiocam 305 camera. Samples were transferred and imaged into a 6-channel microfluidic chamber μ -Slide VI 0.4 polymer coverslip (Ibidi, Germany). Samples containing Cy3, Cy5/AlexaFluor647 and 6-Fam/AlexaFluor488 were visualized at excitation wavelengths of 548, 650 and 493 nm, respectively. The exposure time for image acquisition was set at 150 000 ms for fluorophores conjugated to nanostars and at 20 000 ms for the fluorophore conjugated to the antibody. Imaging was performed at room temperature. For each experiment, 13 images were acquired at each time point in each experimental replica, in order to cover the full surface area of the μ -chambers. Images were initially acquired using a region of interest (ROI) of 2464 × 2056 pixels, while a cropped area of 500 × 500 pixels is reported in figures. Videos are shown with enhanced contrast for better visualization.

Confocal Microscopy. An EVIDENT FV-4000 confocal laser scanning microscope was used to investigate the spatial distribution of Cy3 (biotin–DNA nanostars) and AF647 (anti-biotin antibody) fluorophores within condensates. Fluorescence emission was collected using a 60× oil immersion objective. Images were acquired at three different wavelengths (Laser 488 $\lambda_{\rm ex}$ = 488 nm, $\lambda_{\rm em}$ = 520 nm; Laser 555 HeNe $\lambda_{\rm ex}$ = 555 nm, $\lambda_{\rm em}$ = 572 nm; Laser 635 Diodo $\lambda_{\rm ex}$ = 635 nm, $\lambda_{\rm em}$ = 668 nm).

Image and Data Analysis. Microscope images were exported as Tag Image File Format (.tiff) files. Image analysis was carried out using ImageJ (National Institutes of Health, USA) and custom-made scripts, without applying any LUTs or scaling modifications. Analyses were performed on 10 random microscope images per experimental condition. The density (count/mm²) and the mean diameter/area were calculated for each image. These measurements were repeated across three replicates. Final values were reported as the mean of the replicate averages, with standard deviation representing the variation among replicates. For time-lapse experiments, the mean area/ diameter was calculated for each image corresponding to a specific time point. Standard deviation represents the variation within the sample at a specific time point. Colocalization analysis was performed using the JACoP (Just Another Colocalization Plugin) plugin in ImageJ. Pixel intensities from both channels were extracted and normalized. Pearson's coefficient was calculated using correlation analysis in Prism-GraphPad software. Binding curves were fitted using Prism-GraphPad software with its built-in Hill function. Kinetic curves were fitted using a one phase decay equation in the same software. Normalization of the average condensate area was performed by dividing the mean condensate area at each condition by the mean condensate area measured before the addition of free antigen or papain.

ASSOCIATED CONTENT

Supporting Information

The Supporting Information is available free of charge at https://pubs.acs.org/doi/10.1021/jacs.5c13855.

Additional experimental details and oligonucleotides sequences used; theoretical model, curve fitting, control and supporting experiments (PDF)

Video S1, Formation of antibody–DNA hybrid condensates using 300 nM of biotin–DNA nanostars and 150 nM of anti-biotin antibody; anti-biotin antibody is conjugated to AlexaFluor647 (shown in green) (MP4) Video S2, Confocal z-stack of antibody–DNA hybrid condensates using 300 nM of biotin–DNA nanostars

and 150 nM of anti-biotin antibody; biotin–DNA nanostars are conjugated to Cy3 (shown in red) and anti-biotin antibody is conjugated to AlexaFluor647 (shown in green); from left: Cy3 channel, Cy5 channel, bright field (BF) and merged (MP4)

Video S3, Papain-driven biotin antibody—DNA hybrid condensates dissolution, using 300 nM of biotin—DNA nanostars, 150 nM of anti-biotin antibody and 1.5 μ M of papain; anti-biotin antibody is conjugated to Alexa-Fluor647 (shown in green); left: theoretical simulation, right: experimental result (MP4)

■ AUTHOR INFORMATION

Corresponding Authors

Erica Del Grosso — Department of Chemical Sciences and Technologies, University of Rome, Tor Vergata, 00133 Rome, Italy; Email: Erica.del.grosso@uniroma2.it

Francesco Ricci — Department of Chemical Sciences and Technologies, University of Rome, Tor Vergata, 00133 Rome, Italy; orcid.org/0000-0003-4941-8646; Email: Francesco.ricci@uniroma2.it

Authors

Sara Scalia – Department of Chemical Sciences and Technologies, University of Rome, Tor Vergata, 00133 Rome, Italy

Marco Cappa – Physics Department, Sapienza University of Rome, 00185 Rome, Italy

Lorenzo Rovigatti — Physics Department, Sapienza University of Rome, 00185 Rome, Italy; orcid.org/0000-0001-5017-2829

Complete contact information is available at: https://pubs.acs.org/10.1021/jacs.5c13855

Author Contributions

All authors have given approval to the final version of the manuscript.

Notes

The authors declare no competing financial interest.

ACKNOWLEDGMENTS

This work was supported by the European Research Council, ERC (project n.819160 to F.R.), by Associazione Italiana per la Ricerca sul Cancro, AIRC (project n. 21965) (F.R.) and by the Italian Ministry of University and Research (Project of National Interest, PRIN, 2017YER72K). L.R. acknowledges support from MUR-PRIN Grants No. 20225NPY8P and P2022JZEJR, funded by European Union—NextGenerationEU, Missione 4 Componente 2—CUP B53D23028570001. We thank Dr. Elena Romano, "Patrizia Albertano" Advanced Microscopy Center, Laboratory of Confocal Microscopy, Department of Biology, University of Rome Tor Vergata, for support with the confocal microscopy images. We also thank Lorenzo Di Michele and Fabrizio Camerin for helpful discussions.

REFERENCES

- (1) Seeman, N. C.; Sleiman, H. F. DNA nanotechnology. Nat. Rev. Mater. 2018, 3, No. 17068.
- (2) Jasinski, D.; Haque, F.; Binzel, D. W.; Guo, P. Advancement of the Emerging Field of RNA Nanotechnology. *ACS Nano* **2017**, *11* (2), 1142–1164.

- (3) Abraham, G. R.; Chaderjian, A. S.; N Nguyen, A. B.; Wilken, S.; Saleh, O. A. Nucleic acid liquids. *Rep. Prog. Phys.* **2024**, 87 (6), No. 066601.
- (4) Udono, H.; Gong, J.; Sato, Y.; Takinoue, M. DNA Droplets: Intelligent, Dynamic Fluid. *Adv. Biol.* **2023**, *7*, No. 2200180.
- (5) Hegde, O.; Li, T.; Sharma, A.; Borja, M.; Jacobs, W. M.; Rogers, W. B. Competition between self-assembly and phase separation governs high-temperature condensation of a DNA liquid. *Phys. Rev. Lett.* **2024**, 132, No. 208401.
- (6) Biffi, S.; Cerbino, R.; Bomboi, F.; Paraboschi, E. M.; Asselta, R.; Sciortino, F.; Bellini, T. Phase behavior and critical activated dynamics of limited-valence DNA nanostars. *Proc. Natl. Acad. Sci. U.S.A.* **2013**, 110 (39), 15633–15637.
- (7) Merindol, R.; Loescher, S.; Samanta, A.; Walther, A. Pathway-controlled formation of mesostructured all-DNA colloids and superstructures. *Nat. Nanotechnol.* **2018**, *13*, 730–738.
- (8) Sato, Y.; Takinoue, M. Sequence-dependent fusion dynamics and physical properties of DNA droplets. *Nanoscale Adv.* **2023**, *5*, 1919–1925.
- (9) Jeon, B.-J.; Nguyen, D. T.; Saleh, O. A. Sequence-controlled adhesion and microemulsification in a two-phase system of DNA liquid droplets. *J. Phys. Chem. B* **2020**, 124 (40), 8888–8895.
- (10) Jeon, B.-j.; Nguyen, D. T.; Abraham, G. R.; Conrad, N.; Fygenson, D. K.; Saleh, O. A. Salt-dependent properties of a coacervate-like, self-assembled DNA liquid. *Soft Matter* **2018**, *14*, 7009–7015.
- (11) Conrad, N.; Kennedy, T.; Fygenson, D. K.; Saleh, O. A. Increasing valence pushes DNA nanostar networks to the isostatic point. *Proc. Natl. Acad. Sci. U.S.A.* **2019**, *116* (15), 7238–7243.
- (12) Agarwal, S.; Osmanovic, D.; Klocke, M. A.; Franco, E. The growth rate of DNA condensate droplets increases with the size of participating subunits. *ACS Nano* **2022**, *16* (8), 11842–11851.
- (13) Lee, T.; Do, S.; Lee, J. G.; Kim, D.-N.; Shin, Y. The flexibility-based modulation of DNA nanostar phase separation. *Nanoscale* **2021**, 13 (41), 17638–17647.
- (14) Brady, R. A.; Brooks, N. J.; Cicuta, P.; Di Michele, L. Crystallization of amphiphilic DNA C-stars. *Nano Lett.* **2017**, *17* (5), 3276–3281.
- (15) Agarwal, S.; Osmanovic, D.; Dizani, M.; Klocke, M. A.; Franco, E. Dynamic control of DNA condensation. *Nat. Commun.* **2024**, *15*, No. 1915.
- (16) Maruyama, T.; Gong, J.; Takinoue, M. Temporally controlled multistep division of DNA droplets for dynamic artificial cells. *Nat. Commun.* **2024**, *15*, No. 7397.
- (17) Deng, J.; Walther, A. Programmable ATP-fueled DNA coacervates by transient liquid—liquid phase separation. *Chem.* **2020**, *6* (12), 3329—3343.
- (18) Do, S.; Lee, C.; Lee, T.; Kim, D.-N.; Shin, Y. Engineering DNA-based synthetic condensates with programmable material properties, compositions, and functionalities. *Sci. Adv.* **2022**, *8* (41), No. eabj1771.
- (19) Qin, Y.; Sohn, Y. S.; Li, X.; Nechushtai, R.; Zhang, J.; Tian, H.; Willner, I. Photochemically triggered and autonomous oscillatory pH-modulated transient assembly/disassembly of DNA microdroplet coacervates. *Angew. Chem., Int. Ed.* **2025**, *64*, No. e202415550.
- (20) Qin, Y.; Sohn, Y. S.; Nechushtai, R.; Xia, F.; Huang, F.; Willner, I. Enzyme- and DNAzyme-driven transient assembly of DNA-based phase-separated coacervate microdroplets. *J. Am. Chem. Soc.* **2025**, 147 (19), 16141–16153.
- (21) Liu, W.; Deng, J.; Song, S.; Sethi, S.; Walther, A. A facile DNA coacervate platform for engineering wetting, engulfment, fusion and transient behavior. *Commun. Chem.* **2024**, *7*, No. 100.
- (22) Palombo, G.; Weir, S.; Michieletto, D.; Fosado, Y. A. G. Topological linking determines elasticity in limited valence networks. *Nat. Mater.* **2025**, *24*, 454–461.
- (23) Fabrini, G.; Minard, A.; Brady, R. A.; Di Antonio, M.; Di Michele, L. Cation-responsive and photocleavable hydrogels from noncanonical amphiphilic DNA nanostructures. *Nano Lett.* **2022**, 22 (2), 602–611.

- (24) Zhao, Q. H.; Qi, J. Y.; Deng, N.-N. DNA photofluids show lifelike motion. *Nat. Mater.* **2025**, *24*, 935–944.
- (25) Lu, S.; Wang, S.; Zhao, J.; Sun, J.; Yang, X. A pH-controlled bidirectionally pure DNA hydrogel: reversible self-assembly and fluorescence monitoring. *Chem. Commun.* **2018**, *54*, 4621–4624.
- (26) Um, S. H.; Lee, J.; Park, N.; Kwon, S.; Umbach, C. C.; Luo, D. Enzyme-catalysed assembly of DNA hydrogel. *Nat. Mater.* **2006**, *5*, 797–801.
- (27) Leathers, A.; Walczak, M.; Brady, R. A.; Al Samad, A.; Kotar, J.; Booth, M. J.; Cicuta, P.; Di Michele, L. Reaction—diffusion patterning of DNA-based artificial cells. *J. Am. Chem. Soc.* **2022**, *144* (38), 17468—17476.
- (28) Malouf, L.; Tanase, D. A.; Fabrini, G.; Brady, R. A.; Paez-Perez, M.; Leathers, A.; Booth, M. J.; Di Michele, L. Sculpting DNA-based synthetic cells through phase separation and phase-targeted activity. *Chem* **2023**, *9* (11), 3347–3364.
- (29) Agarwal, S.; Dizani, M.; Osmanovic, D.; Franco, E. Light-controlled growth of DNA organelles in synthetic cells. *Interface Focus* **2023**, *13*, No. 20230017.
- (30) Samanta, A.; Hörner, M.; Liu, W.; Weber, W.; Walther, A. Signal-processing and adaptive prototissue formation in metabolic DNA protocells. *Nat. Commun.* **2022**, *13*, No. 3968.
- (31) Samanta, A.; Pellejero, L. B.; Masukawa, M.; Walther, A. DNA-empowered synthetic cells as minimalistic life forms. *Nat. Rev. Chem.* **2024**, *8*, 454–470.
- (32) Fabrini, G.; Farag, N.; Nuccio, S. P.; Li, S.; Stewart, J. M.; Tang, A. A.; McCoy, R.; Owens, R. M.; Rothemund, P. W. K.; Franco, E.; Di Antonio, M.; Di Michele, L. Co-transcriptional production of programmable RNA condensates and synthetic organelles. *Nat. Nanotechnol.* **2024**, *19*, 1665–1673.
- (33) Dizani, M.; Sorrentino, D.; Agarwal, S.; Stewart, J. M.; Franco, E. Protein recruitment to dynamic DNA-RNA host condensates. *J. Am. Chem. Soc.* **2024**, *146* (43), 29344–29354.
- (34) Stewart, J. M.; Li, S.; Tang, A. A.; Klocke, M. A.; Gobry, M. V.; Fabrini, G.; Di Michele, L.; Rothemund, P. W. K.; Franco, E. Modular RNA motifs for orthogonal phase-separated compartments. *Nat. Commun.* **2024**, *15* (1), No. 6244.
- (35) Bucci, J.; Malouf, L.; Tanase, D. A.; Farag, N.; Lamb, J. R.; Rubio-Sánchez, R.; Gentile, S.; Del Grosso, E.; Kaminski, C. F.; Di Michele, L.; Ricci, F. Enzyme-responsive DNA condensates. *J. Am. Chem. Soc.* **2024**, *146* (46), 31529–31537.
- (36) Kengmana, E.; Ornelas-Gatdula, E.; Chen, K.-L.; Schulman, R. Spatial control over reactions via localized transcription within membraneless DNA nanostar droplets. *J. Am. Chem. Soc.* **2024**, *146* (48), 32942–32952.
- (37) Park, N.; Um, S.; Funabashi, H.; Xu, J.; Luo, D. A cell-free protein-producing gel. *Nat. Mater.* **2009**, *8*, 432–437.
- (38) Dong, J.; Xia, F.; Huang, F.; Willner, I. Dynamic transcription machineries in protocells. *J. Am. Chem. Soc.* **2025**, *147*, 18359–18373.
- (39) Banani, S. F.; Lee, H. O.; Hyman, A. A.; Rosen, M. K. Biomolecular condensates: organizers of cellular biochemistry. *Nat. Rev. Mol. Cell Biol.* **2017**, *18*, 285–298.
- (40) Gomes, E.; Shorter, J. The molecular language of membraneless organelles. *J. Biol. Chem.* **2019**, 294 (18), 7115–7127.
- (41) Hirose, T.; Ninomiya, K.; Nakagawa, S.; Yamazaki, T. A guide to membraneless organelles and their various roles in gene regulation. *Nat. Rev. Mol. Cell Biol.* **2023**, 24, 288–304.
- (42) Shaw, P.; Brown, J. Nucleoli: composition, function, and dynamics. *Plant Physiol.* **2012**, *158*, 44–51.
- (43) Cioce, M.; Lamond, A. I. Cajal bodies: a long history of discovery. *Annu. Rev. Cell Dev. Biol.* **2005**, *21*, 105–131.
- (44) Luo, Y.; Na, Z.; Slavoff, S. A. P-Bodies: Composition, Properties, and Functions. *Biochemistry* **2018**, *57*, 2424–2431.
- (45) Jain, S.; Wheeler, J. R.; Walters, R. W.; Agrawal, A.; Barsic, A.; Parker, R. ATPase-modulated stress granules contain a diverse proteome and substructure. *Cell* **2016**, *164*, 487–498.
- (46) Fei, J.; Jadaliha, M.; Harmon, T. S.; Li, I. T. S.; Hua, B.; Hao, Q.; Holehouse, A. S.; Reyer, M.; Sun, Q.; Freier, S. M.; Pappu, R. V.; Prasanth, K. V.; Ha, T. Quantitative analysis of multilayer

ı

- organization of proteins and RNA in nuclear speckles at super resolution. J. Cell Sci. 2017, 130 (24), 4180–4192.
- (47) Vieregg, J. R.; Lueckheide, M.; Marciel, A. B.; Leon, L.; Bologna, A. J.; Rivera, J. R.; Tirrell, M. V. Oligonucleotide—peptide complexes: phase control by hybridization. *J. Am. Chem. Soc.* **2018**, 140 (5), 1632—1638.
- (48) Fraccia, T. P.; Jia, T. Z. Liquid Crystal Coacervates Composed of Short Double-Stranded DNA and Cationic Peptides. *ACS Nano* **2020**, *14* (11), 15071–15082.
- (49) Garabedian, M. V.; Su, Z.; Dabdoub, J.; Tong, M.; Deiters, A.; Hammer, D. A.; Good, M. C. Protein condensate formation via controlled multimerization of intrinsically disordered sequences. *Biochemistry* **2022**, *61* (22), 2470–2481.
- (50) Dzuricky, M.; Rogers, B. A.; Shahid, A.; Cremer, P. S.; Chilkoti, A. De novo engineering of intracellular condensates using artificial disordered proteins. *Nat. Chem.* **2020**, *12*, 814–825.
- (51) Sato, Y.; Sakamoto, T.; Takinoue, M. Sequence-based engineering of dynamic functions of micrometer-sized DNA droplets. *Sci. Adv.* **2020**, *6* (23), No. eaba3471.
- (52) Conrad, N.; Chang, G.; Fygenson, D. K.; Saleh, O. A. Emulsion imaging of a DNA nanostar condensate phase diagram reveals valence and electrostatic effects. *J. Chem. Phys.* **2022**, *157*, No. 234203.
- (53) Nguyen, D. T.; Saleh, O. A. Tuning phase and aging of DNA hydrogels through molecular design. *Soft Matter* **2017**, *13*, 5421–5427.
- (54) Locatelli, E.; Handle, P. H.; Likos, C. N.; Sciortino, F.; Rovigatti, L. Condensation and demixing in solutions of DNA nanostars and their mixtures. *ACS Nano* **2017**, *11*, 2094–2102.
- (55) Cappa, M.; Sciortino, F.; Rovigatti, L. A phase-field model for solutions of DNA-made particles. *J. Chem. Phys.* **2025**, *162*, No. 194901.
- (56) Sutton, B. J.; Davies, A. M.; Bax, H. J.; Karagiannis, S. N. IgE Antibodies: From Structure to Function and Clinical Translation. *Antibodies* **2019**, 8, No. 19.
- (57) McCraw, A. J.; Palhares, L.; Hendel, J.; Gardner, R.; Santaolalla, A.; Crescioli, S.; McDonnell, J.; van Hemelrijck, M.; Chenoweth, A.; Spencer, D.; Wagner, G.; Karagiannis, S. IgE glycosylation and impact on structure and function: A systematic review. *Allergy* **2024**, *79*, 2625–2661.
- (58) Yu, X.; Sharma, K. D.; Takahashi, T.; Iwamoto, R.; Mekada, E. Ligand-independent dimer formation of epidermal growth factor receptor (EGFR) is a step separable from ligand-induced EGFR signaling. *Mol. Biol. Cell* **2002**, *13* (7), 2547–2557.
- (59) Kim, D.-H.; Kim, D.-K.; Zhou, K.; Park, S.; Kwon, Y.; Jeong, M. G.; Lee, N. K.; Ryu, S. H.; et al. Single particle tracking-based reaction progress kinetic analysis reveals a series of molecular mechanisms of cetuximab-induced EGFR processes in a single living cell. *Chem. Sci.* **2017**, *8* (7), 4823–4832.